



Slow wave and truly rainbow trapping in a one-way terahertz waveguide

JIE XU,^{1,2} PANPAN HE,³ DELONG FENG,^{1,2} KANGLE YONG,^{1,2}
LUJUN HONG,⁴ YUN SHEN,⁴ AND YUN ZHOU^{1,2,*}

¹School of Medical Information and Engineering, Southwest Medical University, Luzhou 646000, China

²Medicine & Engineering & Information Fusion and Transformation Key Laboratory of Luzhou City, Luzhou 646000, China

³Department of Electronic Engineering, Luzhou Vocational and Technical College, Luzhou 646000, China

⁴Institute of Space Science and Technology, Nanchang University, Nanchang 330031, China

*18591988761@163.com

Abstract: Slowing down or even trapping electromagnetic (EM) waves attract researchers' attention for its potential applications in energy storage, optical signal processing and nonlinearity enhancement. However, conventional trapping, in fact, is not truly trapping because of the existence of strong coupling effects and reflections. In this paper, a novel metal-semiconductor-semiconductor-metal (MSSM) heterostructure is presented, and novel truly rainbow trapping of terahertz waves is demonstrated based on a tapered MSSM structure. More importantly, functional devices such as optical buffer, optical switch and optical filter are achieved in one single structure based on the truly rainbow trapping theory. Owing to the property of one-way propagation, these new types of optical devices can be high performance and are expected to be used in integrated optical circuits.

© 2021 Optical Society of America under the terms of the [OSA Open Access Publishing Agreement](#)

1. Introduction

Electromagnetic (EM) waves can propagate in both forward and backward directions in a general physical system because of the presence of the time-reversal symmetry of the system. One-way propagating EM modes, on the other hand, are those EM waves that can only travel in one direction in a physical system, which is similar to the chiral edge state in the quantum Hall effect [1]. The unidirectional EM waves can bypass imperfections as well as bends because they are immune to backscattering. Applying an external magnetic field is one of the fundamental ways to design one-way waveguides [2–7]. The relative permittivity or permeability tensor will be induced in such systems, and, accordingly, Lorentz reciprocity are broken, which will further lead to the nonreciprocal propagation of the EM waves. It was reported that the one-way EM waves are found when an external magnetic field is applied to two-dimensional photonic crystals composed of magneto-optical (MO) materials due to broken time-reversal symmetry [8]. In 2009, the existence of such one-way EM modes was experimentally observed in a photonic crystal consisted of yttrium-iron-garnet (YIG) which is a MO material in microwave regime [9]. One-way EM modes sustained by the interface of dielectric and MO material is called the surface magnetoplasmon (SMP) [10,11], and because of the dc magnetic field, the asymptotic frequencies of SMPs are different in forward and backward. Thus, there are a complete one-way propagating (COWP) band for SMPs [12]. Recently, we presented Y-branch [13] and t-shaped [14] beam splitters based on one-way SMPs. More recently, time-bandwidth limit was reported to be broken in a truncated one-way waveguide in which SMPs are localized and behave as in a 'zero-dimensional' cavity [15] around the terminal.

As is well known, the speed of light is constant, which make it technically impossible to accelerate light. However, slowing light or waves is found to be possible in the past decades. In 1999, an experimental demonstration of slowing the speed of light to 17 metres per second was

present by utilizing a quantum effect called electromagnetically induced transparency (EIT) [16]. In addition to EIT, it was also possible to use photonic crystals (PhCs) or metamaterials to slow light. By tailoring the dispersion properties of light in the photonic bandgaps (PBGs) of PhCs, the group velocity of light can be dramatically decreased [17–21]. In the other hand, metamaterials can possess special properties like negative refractive index, which can also be used in slowing EM waves or light [22]. Graphene, undoubtedly, is in the spotlight today, and graphene-based metamaterials can slow light using the principle of plasmon-induced transparency (PIT) which is similar to EIT [23–25]. Rainbow trapping refers to the capture of EM waves or light of different frequencies at different spatial locations. There are various structures in which the rainbow trapping can be achieved, including three-dimensional photonic crystals with spatially distance between layers changing along the directions of propagation [26], chirped plasmonic waveguide [27], metasurfaces [28], metamaterials [22,29], and one-way waveguides consisting of MO materials [30,31]. Besides, the rainbow trapping and field enhancement effects of acoustic waves were predicted and experimentally demonstrated in several works [32–34].

Rainbow trapping is promising in optical storage, however, due to the coupling between forward and backward EM modes, the slowed down or trapped fields could gradually propagate to opposite direction [35]. The original idea of the truly rainbow trapping came from Ref. [30]. The authors proposed a metal-dielectric-YIG structure and by utilizing a linearly increasing magnetic field, they achieved truly rainbow trapping in microwave regime due to the absence of the coupling effects between forward and backward EM waves. In this paper, we achieve the truly rainbow trapping in terahertz regime based on a novel mechanism in a metal-semiconductor-semiconductor-metal (MSSM) model. Instead of using linearly changing dc magnetic field, we achieve the truly rainbow trapping in a tapered MSSM structure, which makes our model more practical than the one in Ref. [30]. Besides, we further present potential ways to utilize our MSSM model in optical buffer, filter and switch.

2. Three complete one-way propagation bands

The inset of Fig. 1(a) shows the physical model of the metal-semiconductor-semiconductor-metal (MSSM) structure, in which one of semiconductors is assumed to be under an external magnetic field B_0 with -y direction. Because of the existence of B_0 , the time-reversal symmetry in the MSSM waveguide will be broken. We first theoretically study the dispersion and propagation properties of the electromagnetic (EM) waves in the MSSM model. The metal can be treated as perfect electric conductor (PEC) in the terahertz regime [36] and in this paper, the semiconductors are assumed to be indium antimonide (InSb). We emphasize here that the InSb layers are assumed to be lossless in the theoretical analysis because the losses of the system have no significant impact on the one-way propagation property [36–38]. Moreover, to distinguish two layers of InSb, they are named InSb-1 and InSb-2. The upper layer semiconductor (InSb-1) is described by the Drude model, thus its relative permittivity can be written as

$$\epsilon_{\text{Drude}} = \epsilon_{\infty} \left(1 - \frac{\omega_p^2}{\omega^2} \right), \quad (1)$$

where ϵ_{∞} , ω_p and ω are the high-frequency (relative) permittivity, the plasma frequency and the angular frequency, respectively. The relative permittivity of InSb-2, as reported in our earlier paper [31], has off-diagonal tensor form

$$\overset{\leftrightarrow}{\epsilon} = \begin{bmatrix} \epsilon_1 & 0 & i\epsilon_2 \\ 0 & \epsilon_3 & 0 \\ -i\epsilon_2 & 0 & \epsilon_1 \end{bmatrix}, \quad (2)$$

with $\varepsilon_1 = \varepsilon_\infty \left(1 - \frac{\omega_p^2}{\omega^2 - \omega_c^2}\right)$, $\varepsilon_2 = \varepsilon_\infty \frac{\omega_c \omega_p^2}{\omega(\omega^2 - \omega_c^2)}$, $\varepsilon_3 = \varepsilon_\infty \left(1 - \frac{\omega_p^2}{\omega^2}\right)$, where $\omega_c = eB_0/m^*$ is the electron cyclotron frequency. e and m^* are the charge and effective mass of an electron, respectively. Combining Maxwell's equations and all the boundary conditions, one can easily obtain the dispersion equation of surface waves in this MSSM waveguide as written below

$$(k^2 - \varepsilon_1 k_0^2) \tanh(\alpha_s d_2) + \frac{\varepsilon_1}{\varepsilon_{\text{Drude}}} \alpha_D \left[\alpha_s - \frac{\varepsilon_2}{\varepsilon_1} k \tanh(\alpha_s d_2) \right] \tanh(\alpha_D d_1) = 0, \quad (3)$$

where d_1 and d_2 are the thicknesses of the InSb layers. k , k_0 , $\alpha_D = \sqrt{k^2 - \varepsilon_{\text{Drude}} k_0^2}$ and $\alpha_s = \sqrt{k^2 - \varepsilon_v k_0^2}$ ($\varepsilon_v = \varepsilon_1 - \varepsilon_2^2/\varepsilon_1$ is the Voigt permittivity) are the propagation constant, the wavenumber in vacuum, the attenuation coefficient of surface EM waves in InSb-1 and InSb-2, respectively. From Eq. (3) we find $\varepsilon_1 + \varepsilon_{\text{Drude}} - \varepsilon_2 = 0$ for $k \rightarrow +\infty$. Thus, we have

$$2\bar{\omega}^3 - 2\bar{\omega}_c \bar{\omega}^2 - 2\bar{\omega} + \bar{\omega}_c = 0, \quad (4)$$

where $\bar{\omega} = \omega/\omega_p$ and $\bar{\omega}_c = \omega_c/\omega_p$. To analyse the roots of Eq. (4), we set $a = 2$, $b = -2\bar{\omega}_c$, $c = 2$ and $d = \bar{\omega}_c$. By using Shengjin's Formulas, we have $A = b^2 - 3ac = 4\bar{\omega}_c^2 + 12$, $B = bc - 9ad = -14\bar{\omega}_c$ and $C = c^2 - 3bd = 4 + 6\bar{\omega}_c^2$. As a result, the discriminant of Shengjin's Formulas $\Delta = B^2 - 4AC$ remains negative for all values of $\bar{\omega}_c$ and there must be three different solutions for Eq. (4). Further more, the product of three roots equals d and $d = \bar{\omega}_c > 0$, which implies one of the roots must be negative. Therefore, for $k > 0$, there are two asymptotic frequencies (AFs) for SMPs. Likewise, as $k \rightarrow -\infty$, Eq. (3) changes to

$$(2\bar{\omega}^3 + 2\bar{\omega}_c \bar{\omega}^2 - 2\bar{\omega} - \bar{\omega}_c)(\bar{\omega} - \bar{\omega}_c) = 0, \quad (5)$$

$\bar{\omega} = \bar{\omega}_c$ is one of the root of Eq. (5) and for the second form, $\Delta < 0$ and $d = -\bar{\omega}_c < 0$, which indicates that there should be two or four AFs in the MSSM model for $k < 0$. By using numerical calculations, we plot the AFs in Fig. 1(a) as a function of ω_c , and we found that there exist four different AFs in total when $0 < \bar{\omega}_c < 2$. The AFs are named $\omega_{\text{sp}}^{(1)}$, $\omega_{\text{sp}}^{(2)}$, $\omega_{\text{sp}}^{(3)}$ and $\omega_{\text{sp}}^{(4)}$. Such special dispersion property can also be seen in Fig. 1(b), in which $d_1 = d_2 = 0.1\lambda_p$ and $\omega_c = 0.8\omega_p$. The parameters of InSb are $\varepsilon_\infty = 15.6$ and $\omega_p = 4\pi \times 10^{12} \text{ rad}/m$ [39]. In Fig. 1(b), the green coloured zones and the blue dashed curve represent the bulk zones of InSb-2 and InSb-1, respectively. The yellow solid line represent a special kind of SMPs, which is sustained by semiconductor-metal interface, we named it SMs to distinguish from regular SMPs. $\omega_{\text{sp}}^{(1)} = \omega_c$ is the AF of SMs, and the other three horizontal dotted lines in Fig. 1(b) are the AFs of SMPs. The yellow and gray coloured zones are complete one-way propagation (COWP) bands. Note that, when $\omega_c > \omega_0$ ($\omega_0 \approx 0.863\omega_p$) interesting phenomena will appear. However, in this section, we only consider the conditions of $\omega_c < \omega_0$ for studying one-way propagation properties in the MSSM structure.

In our previous work, we found that by cutting off InSb-2 in the vertical direction could significantly enlarge the bandwidth of the COWP band of SMPs [31]. Thus, we plot the dispersion diagram of SMPs for two different values of d_2 in Fig. 2. The thicknesses of InSb-2 are respectively $d_2 = 0.06\lambda_p$ (Fig. 2(a)) and $d_2 = 0.03\lambda_p$ (Fig. 2(b)). The dispersion curves of SMPs in Fig. 2(a) are quite similar to the one in Fig. 1(b), except for the region around $\omega = \omega_p$. The total bandwidth of the COWP bands ($\Delta\omega$) in Fig. 2(a) is obviously large than the one in Fig. 1(b) since the edge of the bulk zone (the green coloured areas) of InSb-2 raised up when d_2 decreased. Note that the COWP-SMs remains the same in Fig. 1(b) and Fig. 2. More interestingly, when d_2 is small enough (e.g. $d_2 = 0.03\lambda_p$), the COWP band of SMPs is divided up into two COWP bands (see Fig. 2(b)), i.e. COWP-1 and COWP-2. The COWP-2 is limited by the cut-off frequency ($\omega_{\text{cf},b}$) of bulk zones of InSb-2 and the cutoff frequency (ω_{cf}) of SMPs for $k \leq 0$. We can not tell from the equations whether $\Delta\omega$ keeps getting bigger as d_2

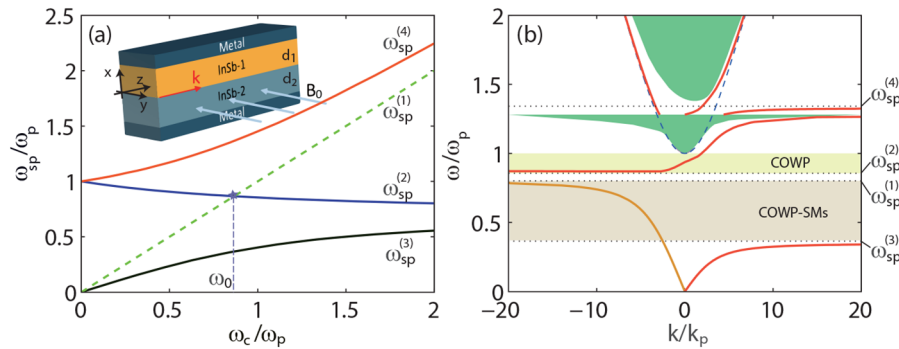


Fig. 1. (a) Four asymptotic frequencies (AFs) of SMPs as functions of ω_c . The inset illustrates the schematic of the metal-semiconductor-semiconductor-metal (MSSM) model. (b) The dispersion diagram of SMPs (red solid lines) and SMs (yellow solid line) as $d_1 = d_2 = 0.1\lambda_p$ and $\omega_c = 0.8\omega_p$. Four horizontal lines represent the AFs and the green shaded areas are the bulk zones in InSb-2.

decrease. To make clear the relation between d_1 , d_2 and $\Delta\omega$, we did numerical calculation as $\omega_c = 0.8\omega_p$ and the results are presented in Fig. 3. In Fig. 3(a), $d_1 = 0.1\lambda_p$ and d_2 is changed from 0 to $0.1\lambda_p$. For $d_1 = d_2 = 0.1\lambda_p$, $\omega_{cf,b} = \omega_p$ and $\omega_{cf}^- < \omega_{sp}^{(2)}$, which fit well with the results shown Fig. 1(b). Moreover, $\Delta\omega$ (red line) will not increase all the time when d_2 decrease, and it reaches a maximum $\Delta\omega_{max} \approx 0.71\omega_p$ around $d_2 = 0.03\lambda_p$. Furthermore, the relation between $\Delta\omega$ and d_1 are also studied for $d_2 = 0.03\lambda_p$. As shown in Fig. 3(b), due to the thin InSb-2, ω_{cf} is constantly larger than $\omega_{sp}^{(2)} = \omega_p$, and $\Delta\omega_{max} \approx 0.79\omega_p$ around $d_1 = 0.03\lambda_p$. We note that the decrease of $\Delta\omega$ as d_1 continue decreasing from $0.03\lambda_p$ is due to the raising up peak of the branch of the dispersion curves of SMPs (e.g. the red line at bottom right of Fig. 2). When designing subwavelength devices with $d_1 < 0.03\lambda_p$, this phenomenon should be considered. However, we just study the structures of $d_1 \geq 0.03\lambda_p$ in this paper.

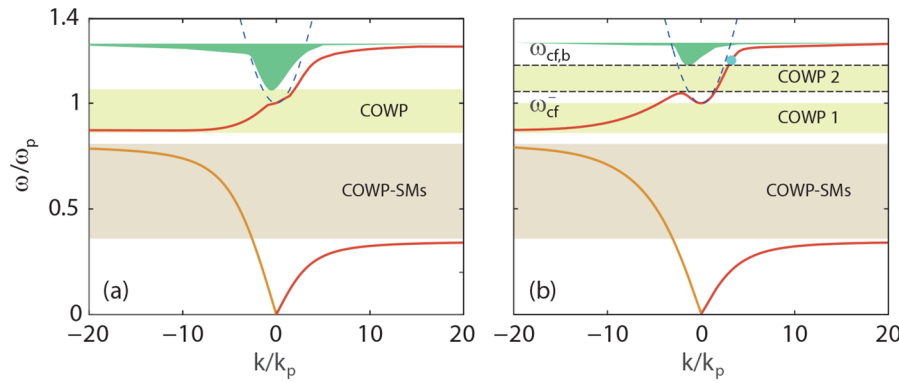


Fig. 2. The dispersion diagram of the MSSM configuration for the cases of (a) $d_2 = 0.06\lambda_p$ and (b) $d_2 = 0.03\lambda_p$. Two shaded yellow areas and the horizontal dashed lines respectively represent the COWP bands of SMPs and the cut-off frequencies of the bulk zone and the dispersion curves as $k \leq 0$. The grey coloured area represents the COWP band of SMs. The other parameters are $d_1 = 0.1\lambda_p$, $\omega_c = 0.8\omega_p$ and $\epsilon_\infty = 15.6$.

Figure 4(a) shows the three COWP bands of the surface EM modes for $d_1 = d_2 = 0.03\lambda_p$ and $\omega_c = 0.8\omega_p$, and three working frequencies (marked by points A, B and C) are chosen to perform

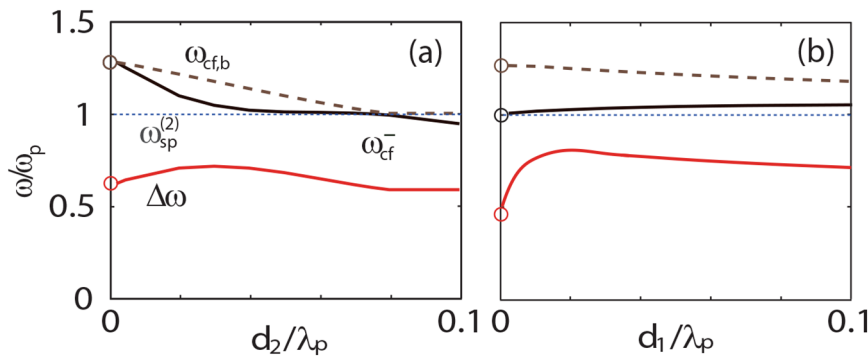


Fig. 3. The total bandwidth $\Delta\omega$ of the COWP bands as functions of (a) d_2 with $d_1 = 0.1\lambda_p$ and (b) d_1 with $d_2 = 0.03\lambda_p$. The other parameters are the same as in Fig. 2.

numerical simulations by using finite element method (FEM). We emphasise here, in this paper, the lossy InSb with the scattering frequency $\nu = 0.001\omega_p$ are considered in numerical simulations.

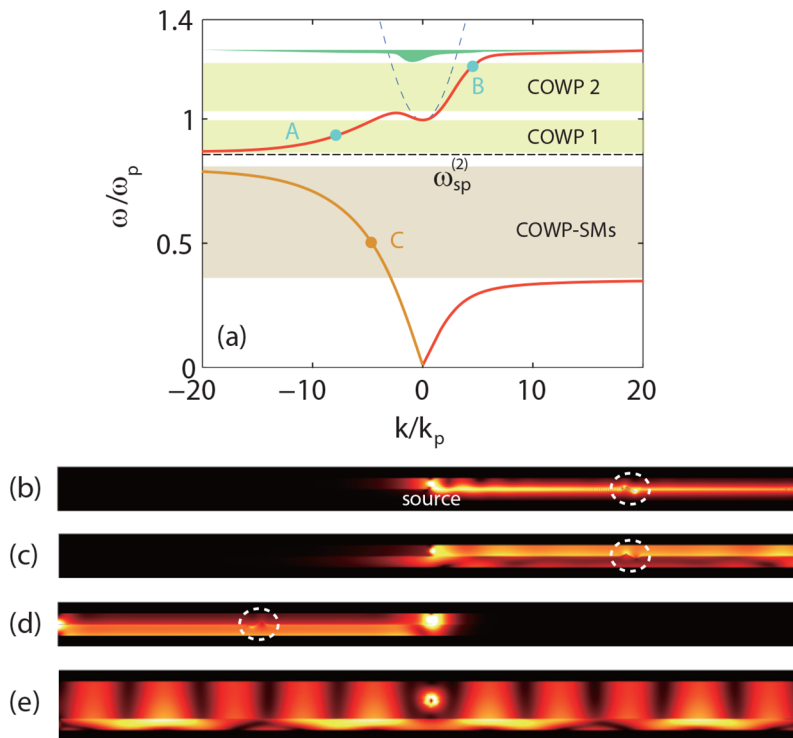


Fig. 4. (a) The dispersion diagram of SMPs and SMs. (b)-(d) The simulated electric field distributions in the MSSM waveguide with 'zig-zag' interfaces emphasized by the white circle for three working frequencies, i.e. (b) $f = 0.9f_p$ (marked by point A in (a)), (c) $f = 1.2f_p$ (marked by point B in (a)) and (d) $f = 0.5f_p$ (marked by point C in (a)). The thickness parameters in (a)-(d) are $d_1 = d_2 = 0.03\lambda_p$. (e) The simulated electric field distribution as $d_2 = 0.1\lambda_p$, $d_1 = 0.03\lambda_p$, and $f = 1.2f_p$ (marked by point in Fig. 2(b)). The other parameters are $\omega_c = 0.8\omega_p$ and the electron scattering frequency of lossy InSb is $\nu = 0.001\omega_p$.

Figures 4(b)-(d) are the simulated electric field distributions as $f = 0.935f_p$ ($f_p = 2$ THz), $f = 1.2f_p$ and $f = 0.5f_p$, respectively. The terminals of the MSSM waveguide are assumed to be PEC wall. As a result, the excited EM waves in Figs. 4(b)-(d) are allowed to propagate in only one direction and no reflection was found in these simulations, which means all three frequencies are in the COWP band. Moreover, for thicker InSb-2 case, e.g. $d_1 = 0.1\lambda_p$, the working frequency $f = 1.2f_p$ will be no longer in the COWP band (see Fig. 2(b)). Figure 4(e) shows the excited EM mode with $f = 1.2f_p$ propagating to both forward and backward direction. We note here that it is the first time the one-way SMs and the one-way (regular) SMPs are simultaneously found in a physical system, and we believe that due to the different characteristics between two unidirectional EM modes, they can be used in different ways, for example, the one-way SMPs can be used to combine the one-way waveguide and the normal dielectric waveguide [36], and the one-way SMs are promising for backscattering immune EM waves propagation and isolation when considering nonlocal effects [38,40,41]. It is worth noting that, in general, nonlocal effects cannot fundamentally destroy the one-way propagation property. The one-way structures can become 'topological' (rather than merely 'unidirectional'), that is, robust to all such material aspects, upon suitable, small modifications of the initial structure [38].

3. Two types of rainbow trapping

Figure 1 tells that when the external magnetic field B_0 is small ($\omega_c < \omega_0$), two kinds of the surface EM modes, i.e. regular SMPs and SMs will not couple with each other for there is a band gap limited by two asymptotic frequencies $\omega_{sp}^{(1)}$ and $\omega_{sp}^{(2)}$. However, once B_0 is large enough ($\omega_c > \omega_0$), the band gap should disappear and new phenomena may appear. For this reason, we studied the dispersion diagrams around the 'gap' as $\omega_c = 0.9\omega_p$. The AFs, in this condition, are respectively $\omega_{sp}^{(1)} = 0.9\omega_p$ and $\omega_{sp}^{(2)} = 0.863\omega_p$. Figure 5 shows the dispersion diagram for four different cases and the according thickness parameters are (a) $d_1 = d_2 = 0.1\lambda_p$, (b) $d_1 = 0.1\lambda_p$, $d_2 = 0.05\lambda_p$, (c) $d_1 = 0.01\lambda_p$, $d_2 = 0.1\lambda_p$, and (d) $d_1 = 0.01\lambda_p$, $d_2 = 0.05\lambda_p$. The strong couple effects of SMPs and SMs can be seen in Fig. 5(a) and (c), in which $d_2 = 0.1\lambda_p$ and the dispersion curves of SMs (the yellow line) and SMPs (the red line) cross each other. More interestingly, slow-wave valley or peak is found in Figs. 5(b) and 5(d), as well as new band gaps. It is obvious that when the thickness of InSb-2 (d_2) decreases from $0.1\lambda_p$ to $0.05\lambda_p$, the dispersion curves of SMs are nearly unchanged and the dispersion curves of SMPs shift up. The unchanged and shift up branches of dispersion curves cause the slow-wave valley (peak) and the band gaps in Figs. 5(b) and 5(d). In addition, as we discussed in Section 2, $d_1 = 0.01\lambda_p$ is not suitable parameter for design and application, we assume $d_1 = 0.1\lambda_p$ for slow-wave and rainbow trapping study.

The thickness-based slow-wave valley can be used to achieve rainbow trapping. Figure 6(a) shows the dispersion diagrams for four different values of d_2 and the solid lines, dashed lines, chain-dotted lines and dotted lines represent the dispersion relation in the MSSM structures with $d_2 = 0.1\lambda_p$, $d_2 = 0.06\lambda_p$, $d_2 = 0.04\lambda_p$ and $d_2 = 0.02\lambda_p$, respectively. It is clearly shown in Fig. 6(a) that, when d_2 decrease from $0.1\lambda_p$ (solid lines) to $0.02\lambda_p$ (dotted lines), the cut-off frequency of SMs (yellow lines) do not change and the slow-wave valley gradually changed to slow-wave peak (red dotted line) with the cut-off frequency shifts up to $\omega_{sp} > \omega_c$ ($\omega_c = \omega_p$). We further designed a straight-tapered joint MSSM waveguide to trap rainbow. As shown in Fig. 6(b), the lengths of the straight and tapered parts of the MSSM waveguide are set to be $L_1 = 150\mu\text{m}$ and $L_2 = 850\mu\text{m}$, respectively. In the tapered part, we set a metal layer (the white dashed line in Fig. 6(b)) in the InSb-2 layer to linearly decrease d_2 . Figures 6(b)-(e) are the electric field distribution of the simulations and, correspondingly, the working frequencies are $f = 0.88f_p$, $f = 0.9f_p$, $f = 0.93f_p$ and $f = 0.95f_p$. One can clearly see the trapped rainbow in Figs. 6(b)-(d) since the EM waves with higher the frequency the longer the trapping length. More visual results are shown in Fig. 6(f), in which the four lines represent the amplitudes of the electric field along the InSb-InSb interface. Unlike the electric field distribution in one-way propagation

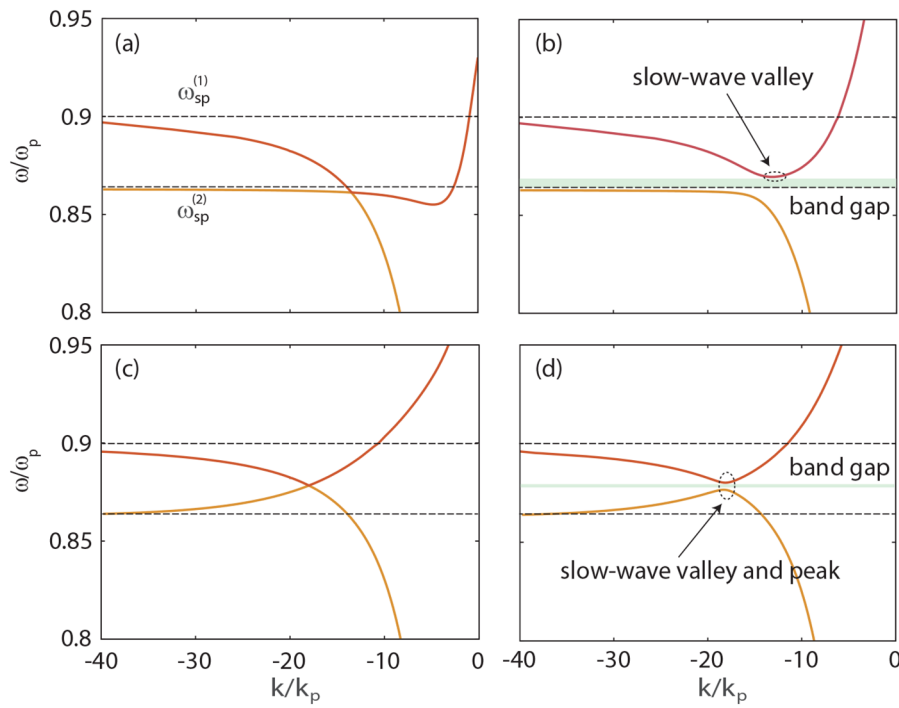


Fig. 5. Zoomed in dispersion diagram of SMPs and SMs when $\omega_c = 0.9\omega_p$ and the thickness parameters are (a) $d_1 = d_2 = 0.1\lambda_p$, (b) $d_1 = 0.1\lambda_p, d_2 = 0.05\lambda_p$, (c) $d_1 = 0.01\lambda_p, d_2 = 0.1\lambda_p$, and (d) $d_1 = 0.01\lambda_p, d_2 = 0.05\lambda_p$. The horizontal lines represent two asymptotic frequencies $\omega_{sp}^{(1)}$ and $\omega_{sp}^{(2)}$. The shaded areas in (b) and (d) are the band gaps of the MSSM waveguide.

cases, the electric fields in Figs. 6(b)-(d) are not uniform and there obviously exist reflections and interference of EM waves in the waveguide. Furthermore, we performed simulations using finite difference time domain (FDTD) method to verify the rainbow trapping in lossy cases with $\nu = 0.001\omega_p$. In the FDTD simulations, a Gause pulse was set to be the source, and the center frequency and the bandwidth of the pulse were $f_0 = 0.92f_p$ and $\Delta\omega = 0.06f_p$, respectively. For simplicity, we set $L = 200\mu\text{m}$ and $L_1 = 50\mu\text{m}$ in our FDTD simulations. As a result, similar trapping phenomenon was observed as shown the inset of Fig. 6(f). Since we have observed the rainbow trapping in both the FEM and the FDTD simulations, it is believable that the slow-wave valley or the valley zero-group-velocity points survived in the lossy cases. On the other hand, the EM waves of the trapped rainbow can be excited by short pulse, which guarantees the robustness of the slow-wave valley in lossy cases [37]. According to the simulation results, this slow-wave valley-induced rainbow trapping has much higher trapping efficiency than the slow-wave peak-induced rainbow trapping reported in our previous work [31] for there are no SMPs for $k > 0$ around slow-wave valley. Note that the tapered MSSM waveguide shown in Fig. 6 may not suitable to design energy storage because of the rainbow trapping effect which will lead to big hotspots of trapped EM waves as shown the inset of Fig. 6(f), and the coupling effects between the EM waves, especially the forward and backward coupling effects [30]. According to the FDTD calculation, the trapped pulse attenuated in the first $\Delta t \approx 40T_p$ ($T_p = 1/f_p$) after trapping and Δt is about 2.4 times of $1/\Delta\omega$. Therefore, the proposed tapered MSSM configuration is suitable to design optical devices such as optical filter rather than energy storage. Besides, such straight-tapered joint MSSM configuration can also be used to achieve truly rainbow trapping.

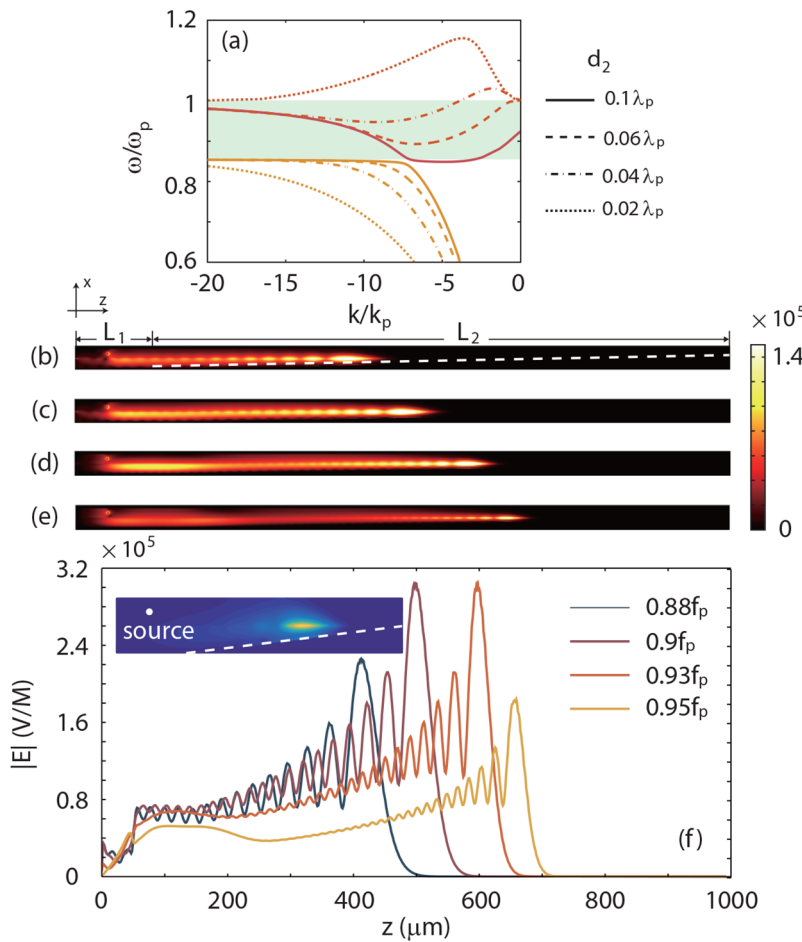


Fig. 6. (a) The dispersion curves of surface waves for four different value of d_2 as $d_1 = 0.1\lambda_p$ and $\omega_c = \omega_p$. (b)-(e) Simulated electric field amplitudes in a tapered MSSM configuration for (b) $f = 0.88f_p$, (c) $f = 0.9f_p$, (d) $f = 0.93f_p$ and (e) $f = 0.95f_p$. The lengths of the straight and tapered parts of the MSSM waveguide are respectively $L_1 = 150\mu\text{m}$ and $L_2 = 850\mu\text{m}$, and the thickness parameters of the straight part are $d_1 = d_2 = 0.1\lambda_p$. (f) The electric field amplitude distributions along the InSb-InSb interfaces in (b), (c), (d) and (e). The inset of (f) shows the electric field distribution in the FDTD simulations.

The concept of truly trapped rainbow comes from Ref. [35], in which the researcher illustrates the coupling between forward and backward propagating EM modes in a tapered metamaterial waveguide will greatly influence the process of rainbow capture. The critical problem in truly rainbow trapping is how to overcome the forward-backward coupling. Here, we propose a novel truly rainbow trapping theory based on the MSSM configuration. Figure 5 and Fig. 6(a) show that once $\omega_c > \omega_0$ the dispersion curves of SMPs (red lines) will shift up with the decrease of d_2 . When d_2 is small enough, the dispersion curves of SMPs can 'escape' to $\omega > \omega_{sp}^{(1)}$ region (e.g. red dotted line in Fig. 6(a)). Much more interestingly, $\omega = \omega_{sp}^{(1)}$ appears to be a solution of Eq. (3) in all cases. Figures 7(a) and 7(b) provide a more clear description of truly rainbow trapping theory, in which the parameters are $d_1 = 0.1\lambda_p$ and $\omega_{sp}^{(1)} = \omega_c = 0.9\omega_p$. Four types of lines represent four values of d_2 and they are respectively $d_2 = 0.1\lambda_p$ (solid line), $d_2 = 0.03\lambda_p$ (dash line) and $d_2 = 0.02\lambda_p$ (chain-dotted line). It is quite clear that $f/f_p = \omega_{sp}^{(1)}/\omega_p$ (black

points in Fig. 7(a)) holds in three conditions, which means the EM waves with $f = \omega_{sp}^{(1)}/\omega_p \cdot f_p$ can propagate in the corresponding structures and are prohibited in the case of $d_2 = 0.01\lambda_p$. Based on this theory, we perform full wave simulations in the same waveguide as the one in Fig. 6(b). In Figs. 7(c)-(f), the working frequencies f and the electron cyclotron frequency ω_c satisfied the equation $f/f_p = \omega_c/\omega_p$. Four working frequencies are the same with those in Figs. 6(b)-(e). As shown in Figs. 7(c)-(f), the EM waves with different frequencies are trapped at different locations and, excitingly, the electric fields in all simulations have uniform distributions. Figure 7(g) indicates the according amplitude of the electric field along the InSb-InSb interface in the simulations and there is nearly no reflection and interference. Comparing with the trapped rainbow mentioned in Fig. 6, the rainbow in Fig. 7 is truly trapped for the trapped EM waves can not travel in the reverse direction. It should also be noted that the truly rainbow trapping mechanism is not applicable to energy storage, since the changing external magnetic field will destroy the storing or trapping of the EM waves.

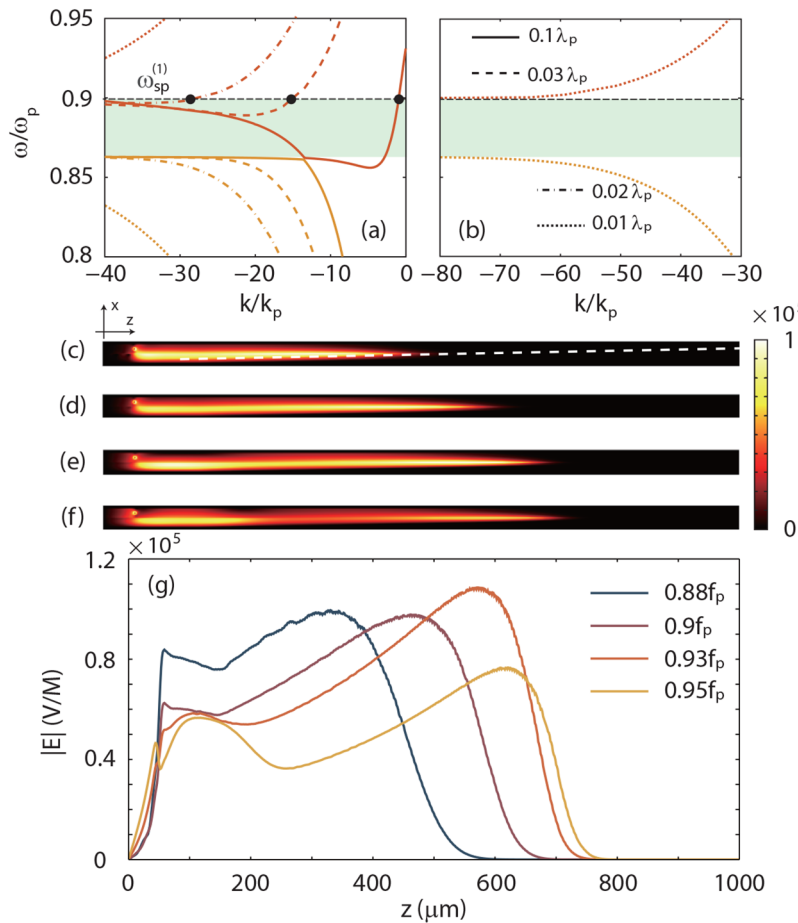


Fig. 7. Truly rainbow trapping. (a), (b) The dispersion diagrams for four different d_2 (as shown the inset of (b)). The other parameters are $d_1 = 0.1\lambda_p$ and $\omega_c = 0.9\omega_p$. (c)-(f) The simulated electric field distribution in the same tapered structure as in Fig. 6(b). $f/f_p = \omega_c/\omega_p$ and the working frequencies in (c)-(f) are the same as in Figs. 6(b)-(e). (g) The electric field amplitudes distribution along the InSb-InSb interfaces in (c), (d), (e) and (f).

4. Optical filter, switch, and buffer based on the MSSM configuration

Compared with the conventional trapping, the truly trapped EM waves can neither reflect nor couple with the bulk modes [38]. Therefore, such truly rainbow trapping devices can achieve significant field enhancement [15,30,42], and has many potential applications in photon harvesting [43], detector [44], near-field fluorescence imaging [45], optical signal processing [46] and optical nonlinearity enhancement [47]. In this section, we design an optical device which can be used as an optical buffer, optical filter and optical switch as well. We first study the relation between d_2 and ω_c as $d_1 = 0.1\lambda_p$ under the condition of $f/f_p = \omega_c/\omega_p$. For truly trapping rainbow, the external magnetic field must be relatively large, more specifically, $\omega_c > \omega_0$. Thus, in this section, we only consider $0.87\omega_p \leq \omega_c \leq \omega_p$. In Fig. 8(a), the $d_2 - \omega_c$ space is splitted into two areas by the red line which is the fitted curve of numerical solutions (marked by stars) of Eq. (3) when truly trapping rainbow happens. The yellow coloured area and the orange coloured area are named the releasing zone and the trapping zone. Points located in the trapping or releasing zone implies the EM waves with $f = \omega_c/\omega_p \cdot f_p$ can or can not be trapped in the corresponding condition. Moreover, the y axis of Fig. 8(a), the vertical dashed line, the horizontal dashed line and the x axis of Fig. 8(a) represent $\omega_c = 0.87\omega_p$, $\omega_c = 0.935\omega_p$, $d_2 = 0.015\lambda_p$ and $d_2 = 0.01\lambda_p$. According to the zones of trapping and releasing, the black or the red point implies that, when $f/f_p = \omega_c/\omega_p$, the EM waves can be trapped at the location with $d_2 = 0.015\lambda_p$ or $d_2 = 0.01\lambda_p$. On the other

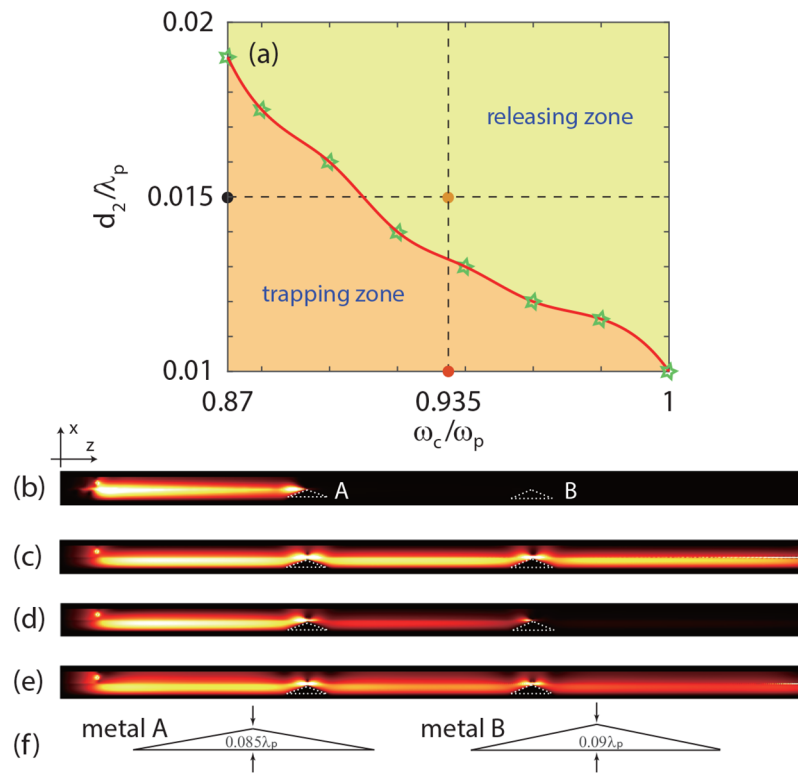


Fig. 8. (a) The mechanism of trapping and releasing the EM wave based on $f/f_p = \omega_c/\omega_p$. (b)-(e) The numerical simulations in a MSSM structure with two metal barriers A and B (the white lines) for (b) $f = 0.87f_p$ and $\omega_c = 0.87\omega_p$, (c) $f = 0.935f_p$ and $\omega_c = 0.87\omega_p$, (d) $f = 0.935f_p$ and $\omega_c = 0.935\omega_p$ and (e) $f = 0.95f_p$ and $\omega_c = 0.935\omega_p$. (f) The schematic of metal barriers. In the straight part of the waveguide, the thickness parameters are $d_1 = d_2 = 0.1\lambda_p$.

hand, the orange point means the EM waves cannot be trapped in such case. Thus, by carefully designing the thickness of the InSb-2 layer and by controlling the external magnetic field, we can trap or release the EM waves with specific frequencies in a MSSM model. Figures 8(b)-(d) shows the full wave simulations results in a MSSM waveguide with two triangular metal barriers (white lines) A and B which are put on the bottom metal layer of the MSSM waveguide. The positions of the source, peaks of metals A and B are $z = 50\mu\text{m}$, $z = 330\mu\text{m}$ and $z = 630\mu\text{m}$, respectively. $d_1 = d_2 = 0.1\lambda_p$ in the straight part of the MSSM waveguide. Moreover, the height of two metal barriers are $0.085\lambda_p$ and $0.09\lambda_p$, respectively, corresponding to $d_2 = 0.015\lambda_p$ (the horizontal line in Fig. 8(a)) and $d_2 = 0.01\lambda_p$ (the x axis of Fig. 8(a)). In Fig. 8(b), we set $f/f_p = \omega_c/\omega_p = 0.87$. As a result, the excited EM wave is trapped before it encounters the peak of metal A. Comparing with Fig. 8(b), the external magnetic field in Fig. 8(c) remain the same, however, the exciting frequency is changed to $f = 0.935f_p$. In this condition, the excited EM wave propagates through the waveguide instead of being trapped. It can be understand for the asymptotic frequency $\omega_{sp}^{(1)} = \omega_c$ and there are constantly SMPs with $f > \omega_{sp}^{(1)}$ when $\omega_c > \omega_0$ (see Fig. 5, Fig. 6(a) and Fig. 7(a)). More interestingly, when enlarge the external magnetic field and let $f/f_p = \omega_c/\omega_p = 0.935$, the simulation results in Fig. 8(d) show the excited EM wave is trapped around metal B. In addition, Fig. 8(e) shows the EM waves with higher frequency than $0.935f_p$, similar to Fig. 8(c), can not be trapped in the MSSM waveguide when $\omega_c = 0.935\omega_p$. The simulation results shown in Figs. 8(b) and 8(d) fit well with the numerical calculation in Fig. 8(a).

Due to the ability of trapping EM waves with different frequencies at different location, our designed MSSM waveguide shown in Fig. 8 can be treated as an optical filter, besides, it can also be used as an optical switch or optical buffer. Figure 9 shows the potential functions of the MSSM structure. First, as an optical filter, the top diagram of Fig. 9 shows that by carefully designing $d_2^{(1)}$ and $d_2^{(2)}$, the EM wave with lower frequency (f_1) can be trapped while the EM wave with higher frequency (f_2) propagate through the structure. Then, as an optical switch, the last two diagrams of Fig. 9 indicate that the value of ω_c controls the propagation ('on') or capture ('off') of the EM wave with $f = f_2$. Finally, the function of optical buffer can be achieved based on the function of optical switch by controlling the time difference ($\Delta\tau$) between $\omega_c = \omega_c^{(1)}$ and $\omega_c = \omega_c^{(2)}$. The above analysis of optical functional devices can find the according simulations in Fig. 8 when assume $f_1 = 0.87f_p$, $f_2 = 0.935f_p$, $d_2^{(1)} = 0.1\lambda_p$, $d_2^{(2)} = 0.015\lambda_p$, $d_2^{(3)} = 0.01\lambda_p$, $\omega_c^{(1)} = 0.87\omega_p$ and $\omega_c^{(2)} = 0.935\omega_p$. Moreover, due to the one-way propagation properties of the

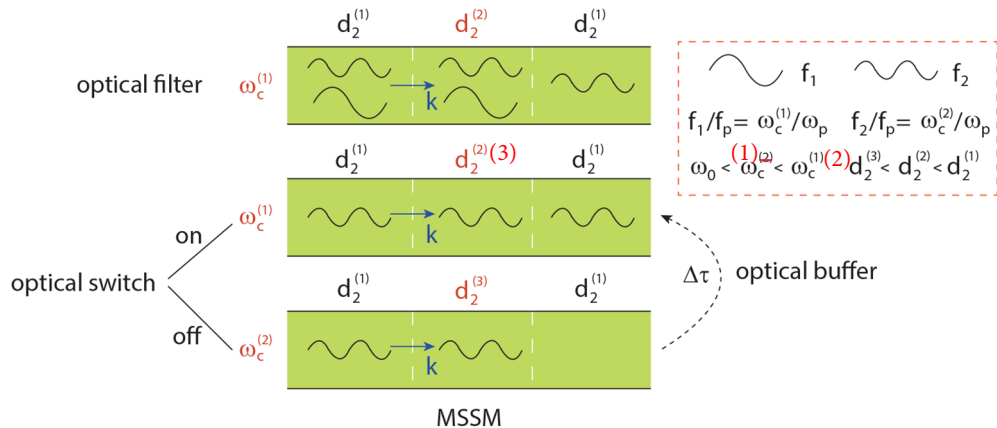


Fig. 9. Realization of optical filter, optical switch and optical buffer based on the MSSM configuration.

EM waves, our proposed optical functional devices based on the MSSM configuration should possess much higher efficiency than regular ones.

5. Conclusion

In conclusion, we have proposed a novel metal-semiconductor-semiconductor-metal (MSSM) model with only one of the semiconductor layer is under an external magnetic field B_0 . In our theoretical analysis, we have shown a special three complete one-way propagation (COWP) bands including two COWP bands of surface magnetoplasmons (SMPs) and one COWP band of surface EM modes (SMs) supported by the semiconductor-metal interface. The simultaneously exist one-way SMPs and one-way SMs are promising for designing optical integrated circuit and for the study of nonlocality. Moreover, by controlling the values of B_0 and the thicknesses of semiconductors, we found slow-wave valley of the dispersion curves of SMPs in the MSSM waveguide. Accordingly, slow-wave valley-based rainbow trapping have been achieved and, more interestingly, new truly rainbow trapping theory was proposed when the electron cyclotron frequency ω_c being larger than a specific value ω_0 (in this paper, $\omega_0 \approx 0.863\omega_p$). By using the finite element method, we further verified the two kinds of rainbow trapping and as a result, the slow-wave valley-based rainbow trapping shows much less reflection than the slow-wave peak-based rainbow trapping reported in our previous work. In the meanwhile, it is the first time that the truly rainbow trapping is achieved in the terahertz regime by simply engineering the thickness of the waveguide. Besides, we also showed the potential uses of our proposed MSSM waveguide in optical filter, optical switch and optical buffer.

Funding. National Natural Science Foundation of China (61865009, 61927813); Department of Science and Technology of Sichuan Province (14JC0153); Science and Technology Strategic Cooperation Programs of Luzhou Municipal People's Government and Southwest Medical University (2019LZXNYDJ18).

Disclosures. The authors declare that there are no conflicts of interest related to this article.

References

1. R. E. Prange and S. M. Girvin, *The Quantum Hall effect* (Springer, 1987).
2. Z. Wang, Y. Chong, J. D. Joannopoulos, and M. Soljačić, "Reflection-free one-way edge modes in a gyromagnetic photonic crystal," *Phys. Rev. Lett.* **100**(1), 013905 (2008).
3. X. Ao, Z. Lin, and C. Chan, "One-way edge mode in a magneto-optical honeycomb photonic crystal," *Phys. Rev. B* **80**(3), 033105 (2009).
4. Z. Yu, G. Veronis, Z. Wang, and S. Fan, "One-way electromagnetic waveguide formed at the interface between a plasmonic metal under a static magnetic field and a photonic crystal," *Phys. Rev. Lett.* **100**(2), 023902 (2008).
5. B. Hu, Q. J. Wang, and Y. Zhang, "Broadly tunable one-way terahertz plasmonic waveguide based on nonreciprocal surface magneto plasmons," *Opt. Lett.* **37**(11), 1895–1897 (2012).
6. S. Pakniyat, A. M. Holmes, G. W. Hanson, S. A. H. Gangaraj, M. Antezza, M. G. Silveirinha, S. Jam, and F. Monticone, "Non-reciprocal, robust surface plasmon polaritons on gyrotropic interfaces," *IEEE Trans. Antennas Propag.* **68**(5), 3718–3729 (2020).
7. S. A. H. Gangaraj, G. W. Hanson, M. G. Silveirinha, K. Shastri, M. Antezza, and F. Monticone, "Unidirectional and diffractionless surface plasmon polaritons on three-dimensional nonreciprocal plasmonic platforms," *Phys. Rev. B* **99**(24), 245414 (2019).
8. S. Raghu and F. D. M. Haldane, "Analogs of quantum-hall-effect edge states in photonic crystals," *Phys. Rev. A* **78**(3), 033834 (2008).
9. Z. Wang, Y. Chong, J. D. Joannopoulos, and M. Soljačić, "Observation of unidirectional backscattering-immune topological electromagnetic states," *Nature* **461**(7265), 772–775 (2009).
10. J. Brion, R. Wallis, A. Hartstein, and E. Burstein, "Theory of surface magnetoplasmons in semiconductors," *Phys. Rev. Lett.* **28**(22), 1455–1458 (1972).
11. R. Wallis, J. Brion, E. Burstein, and A. Hartstein, "Theory of surface polaritons in anisotropic dielectric media with application to surface magnetoplasmons in semiconductors," *Phys. Rev. B* **9**(8), 3424–3437 (1974).
12. L. Shen, Y. You, Z. Wang, and X. Deng, "Backscattering-immune one-way surface magnetoplasmons at terahertz frequencies," *Opt. Express* **23**(2), 950–962 (2015).
13. J. Zou, Y. You, X. Deng, L. Shen, J.-J. Wu, and T.-J. Yang, "High-efficiency tunable y-branch power splitters at terahertz frequencies," *Opt. Commun.* **387**, 153–156 (2017).

14. L. Hong, S. Xiao, X. Deng, R. Pu, and L. Shen, "High-efficiency tunable t-shaped beam splitter based on one-way waveguide," *J. Opt.* **20**(12), 125002 (2018).
15. K. Tsakmakidis, L. Shen, S. Schulz, X. Zheng, J. Upham, X. Deng, H. Altug, A. Vakakis, and R. Boyd, "Breaking lorentz reciprocity to overcome the time-bandwidth limit in physics and engineering," *Science* **356**(6344), 1260–1264 (2017).
16. L. V. Hau, S. E. Harris, Z. Dutton, and C. H. Behroozi, "Light speed reduction to 17 metres per second in an ultracold atomic gas," *Nature* **397**(6720), 594–598 (1999).
17. S. Schulz, L. O'Faolain, D. M. Beggs, T. P. White, A. Melloni, and T. F. Krauss, "Dispersion engineered slow light in photonic crystals: a comparison," *J. Opt.* **12**(10), 104004 (2010).
18. S. Ek, P. Lunnemann, Y. Chen, E. Semenova, K. Yvind, and J. Mork, "Slow-light-enhanced gain in active photonic crystal waveguides," *Nat. Commun.* **5**(1), 5039 (2014).
19. S. A. Schulz, J. Upham, L. O'Faolain, and R. W. Boyd, "Photonic crystal slow light waveguides in a kagome lattice," *Opt. Lett.* **42**(16), 3243–3246 (2017).
20. M. C. Muñoz, A. Y. Petrov, L. O'Faolain, J. Li, T. F. Krauss, and M. Eich, "Optically induced indirect photonic transitions in a slow light photonic crystal waveguide," *Phys. Rev. Lett.* **112**(5), 053904 (2014).
21. S. Yan, X. Zhu, L. H. Frandsen, S. Xiao, N. A. Mortensen, J. Dong, and Y. Ding, "Slow-light-enhanced energy efficiency for graphene microheaters on silicon photonic crystal waveguides," *Nat. Commun.* **8**(1), 14411 (2017).
22. K. L. Tsakmakidis, A. D. Boardman, and O. Hess, "'trapped rainbow' storage of light in metamaterials," *Nature* **450**(7168), 397–401 (2007).
23. S. Zhang, D. A. Genov, Y. Wang, M. Liu, and X. Zhang, "Plasmon-induced transparency in metamaterials," *Phys. Rev. Lett.* **101**(4), 047401 (2008).
24. B. Zhang, H. Li, H. Xu, M. Zhao, C. Xiong, C. Liu, and K. Wu, "Absorption and slow-light analysis based on tunable plasmon-induced transparency in patterned graphene metamaterial," *Opt. Express* **27**(3), 3598–3608 (2019).
25. E. Gao, Z. Liu, H. Li, H. Xu, Z. Zhang, X. Zhang, X. Luo, C. Xiong, C. Liu, B. Zhang, and F. Zhou, "Dual dynamically tunable plasmon-induced transparency in h-type-graphene-based slow-light metamaterial," *J. Opt. Soc. Am. A* **36**(8), 1306–1311 (2019).
26. Z. Hayran, H. Kurt, and K. Staliunas, "Rainbow trapping in a chirped three-dimensional photonic crystal," *Sci. Rep.* **7**(1), 3046 (2017).
27. L. Chen, G. P. Wang, Q. Gan, and F. J. Bartoli, "Rainbow trapping and releasing by chirped plasmonic waveguides at visible frequencies," *Appl. Phys. Lett.* **97**(15), 153115 (2010).
28. Z. Xu, J. Shi, R. J. Davis, X. Yin, and D. F. Sievenpiper, "Rainbow trapping with long oscillation lifetimes in gradient magnetoinductive metasurfaces," *Phys. Rev. Appl.* **12**(2), 024043 (2019).
29. H. Hu, D. Ji, X. Zeng, K. Liu, and Q. Gan, "Rainbow trapping in hyperbolic metamaterial waveguide," *Sci. Rep.* **3**(1), 1249 (2013).
30. K. Liu and S. He, "Truly trapped rainbow by utilizing nonreciprocal waveguides," *Sci. Rep.* **6**(1), 30206 (2016).
31. J. Xu, S. Xiao, C. Wu, H. Zhang, X. Deng, and L. Shen, "Broadband one-way propagation and rainbow trapping of terahertz radiations," *Opt. Express* **27**(8), 10659–10669 (2019).
32. V. Romero-García, R. Picó, A. Cebrero, V. J. Sánchez-Morillo, and K. Staliunas, "Enhancement of sound in chirped sonic crystals," *Appl. Phys. Lett.* **102**(9), 091906 (2013).
33. A. Khelif, A. Choujaa, B. Djafari-Rouhani, M. Wilm, S. Ballandras, and V. Laude, "Trapping and guiding of acoustic waves by defect modes in a full-band-gap ultrasonic crystal," *Phys. Rev. B* **68**(21), 214301 (2003).
34. J. Zhu, Y. Chen, X. Zhu, F. J. Garcia-Vidal, X. Yin, W. Zhang, and X. Zhang, "Acoustic rainbow trapping," *Sci. Rep.* **3**(1), 1728 (2013).
35. S. He, Y. He, and Y. Jin, "Revealing the truth about 'trapped rainbow' storage of light in metamaterials," *Sci. Rep.* **2**(1), 583 (2012).
36. L. Shen, J. Xu, Y. You, K. Yuan, and X. Deng, "One-way electromagnetic mode guided by the mechanism of total internal reflection," *IEEE Photonics Technol. Lett.* **30**(2), 133–136 (2018).
37. K. L. Tsakmakidis, O. Hess, R. W. Boyd, and X. Zhang, "Ulraslow waves on the nanoscale," *Science* **358**(6361), eaan5196 (2017).
38. K. L. Tsakmakidis, Y. You, T. Stefański, and L. Shen, "Nonreciprocal cavities and the time-bandwidth limit: comment," *Optica* **7**(9), 1097–1101 (2020).
39. T. H. Isaac, W. L. Barnes, and E. Hendry, "Determining the terahertz optical properties of subwavelength films using semiconductor surface plasmons," *Appl. Phys. Lett.* **93**(24), 241115 (2008).
40. S. A. H. Gangaraj and F. Monticone, "Do truly unidirectional surface plasmon-polaritons exist?" *Optica* **6**(9), 1158–1165 (2019).
41. S. A. H. Gangaraj and F. Monticone, "Physical violations of the bulk-edge correspondence in topological electromagnetism," *Phys. Rev. Lett.* **124**(15), 153901 (2020).
42. J. Xu, X. Deng, H. Zhang, C. Wu, M. Wubs, S. Xiao, and L. Shen, "Ultra-subwavelength focusing and giant magnetic-field enhancement in a low-loss one-way waveguide based on remanence," *J. Opt.* **22**(2), 025003 (2020).
43. Y. Cui, K. H. Fung, J. Xu, H. Ma, Y. Jin, S. He, and N. X. Fang, "Ultrabroadband Light Absorption by a Sawtooth Anisotropic Metamaterial Slab," *Nano Lett.* **12**(3), 1443–1447 (2012).
44. A. Akbari, R. N. Tait, and P. Berini, "Surface plasmon waveguide Schottky detector," *Opt. Express* **18**(8), 8505–8514 (2010).

45. H. F. Hamann, A. Gallagher, and D. J. Nesbitt, "Near-field fluorescence imaging by localized field enhancement near a sharp probe tip," *Appl. Phys. Lett.* **76**(14), 1953–1955 (2000).
46. A. Krasavin and A. Zayats, "Photonic signal processing on electronic scales: electro-optical field-effect nanoplasmonic modulator," *Phys. Rev. Lett.* **109**(5), 053901 (2012).
47. S. A. H. Gangaraj, B. Jin, C. Argyropoulos, and F. Monticone, "Broadband field enhancement and giant nonlinear effects in terminated unidirectional plasmonic waveguides," *Phys. Rev. Appl.* **14**(5), 054061 (2020).